A.

Upregulated Genes	Downregulated Genes
Complement activation and acute phase response:	
c3b	*ace2*
c3c	*fads2*
c6	*hpx*
cfb	*krt1-19d*
LOC562579	*pvalb8*
LOC792364	*vangl2*
LOC792472	*histone H4*
Cytokines and chemokines:	*zgc:110712*
il1b	*zgc:5594*
LOC100003911	*zgc56053*
LOC562246	*zgc:66382*
tnfb	*zgc:73075*
Defense response:	*zgc:92658*
mpx	
Proteolysis	
ctsc	
tctsh	
ctsl1a	
ctssb2	
mmp13	
mmp9	
npsn	
psma6b	
Transcriptional activation or repression:	
irf11	
irf9	
junb	
LOC100001075	
LOC569187	

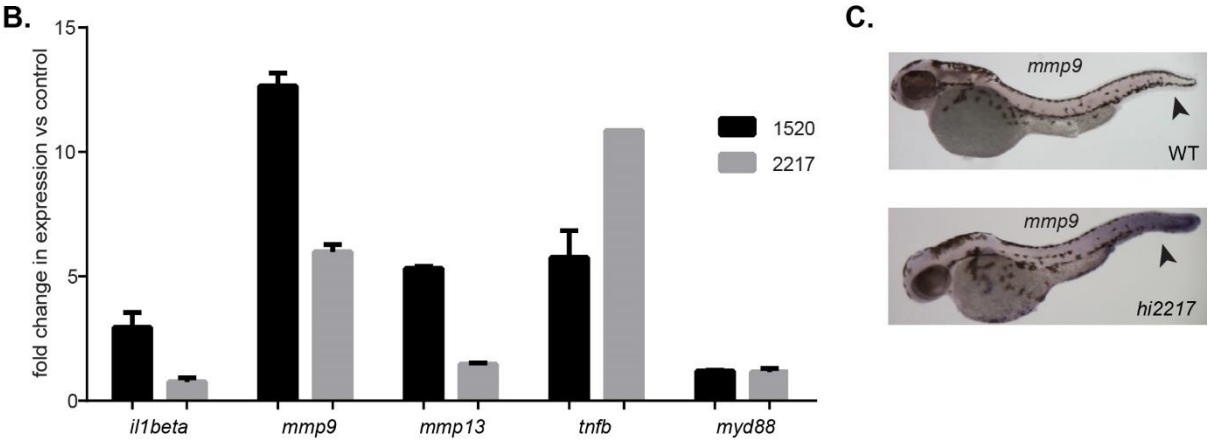

Fig. S1. Inflammation-related gene expression changes are observed in the chronic inflammation mutants *hi2217* and *hi1520*. A) Microarray analysis revealed many inflammation-related genes that were differentially expressed in both inflammation mutants. For a complete list, see GSE28110. B) Confirmation of selected microarray target genes by qRT-PCR confirmed *mmp9* to be highly overexpressed in both of the inflammation mutants. C) In situ hybridization of *mmp9* (arrowhead) in the *hi2217* mutants. For qRT-PCR expression analysis, expression was normalized to *ef1α* expression.

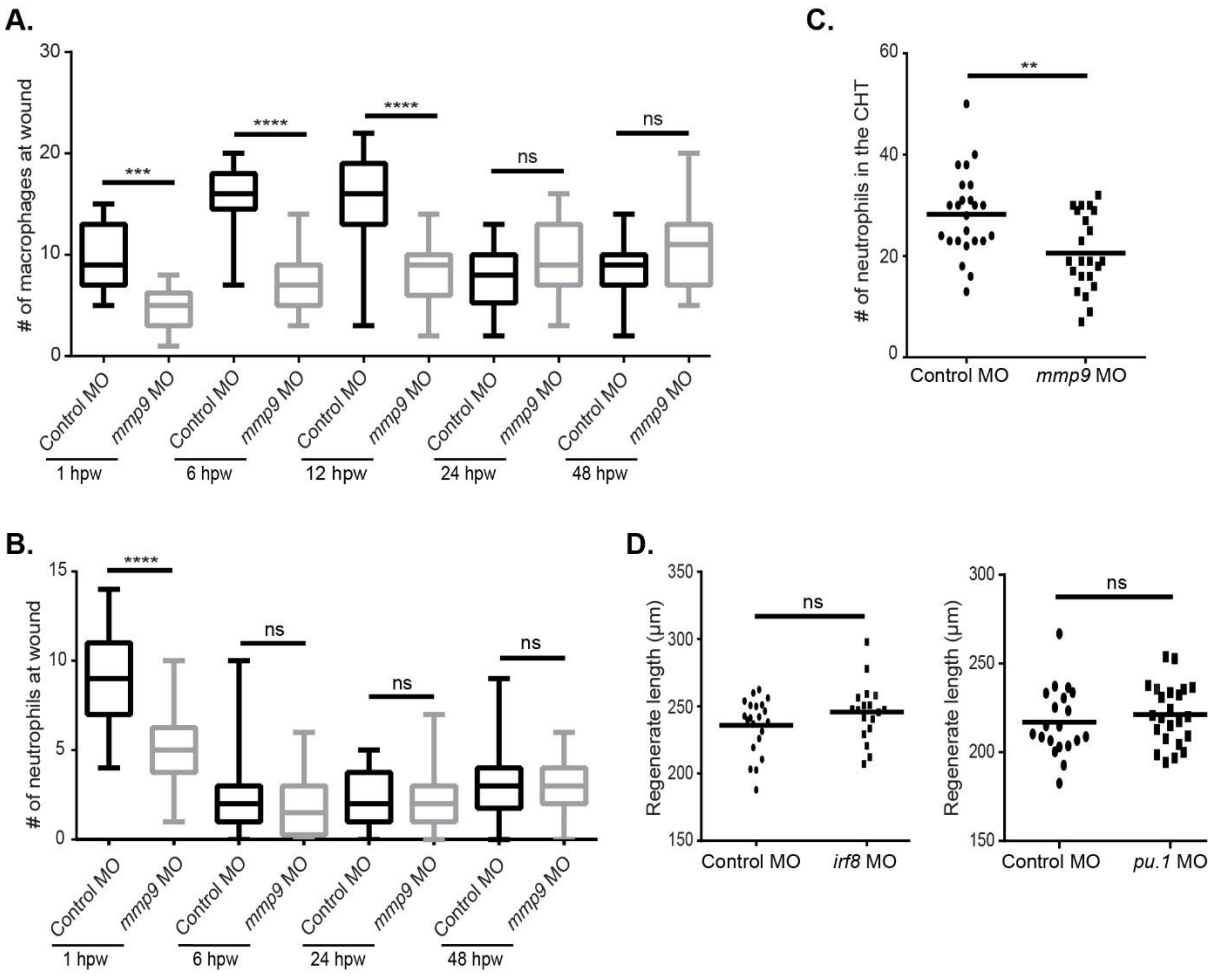

Fig. S2. Knockdown of *mmp9* expression inhibits early leukocyte recruitment to the wound following caudal-fin amputation but does not cause chronic inflammation. A) The *mmp9* morphants displayed reduced macrophage recruitment (1-, 6-, 12 hpw) without influencing inflammation resolution at 24 and 48 hpw. B) Reduced neutrophil recruitment (1 hpw) was also observed in the morphants with no delay in inflammation at later time points. C) Total neutrophil counts in the CHT of unwounded larvae at 2 dpf. D) Macrophage-deficient embryos (*irf8* MO) did not display a wound-healing defect at 3 dpw. Depletion of both neutrophils and macrophages (*pu.1* MO) also resulted in no observable defect in regenerate length at 3 dpw. Statistical significance: * P<0.05, ** P<0.01, *** P<0.001 and ****P<0.0001. Section A represents pooled data from experiments performed in triplicate; B and C are representations from a single experiment performed in triplicate.

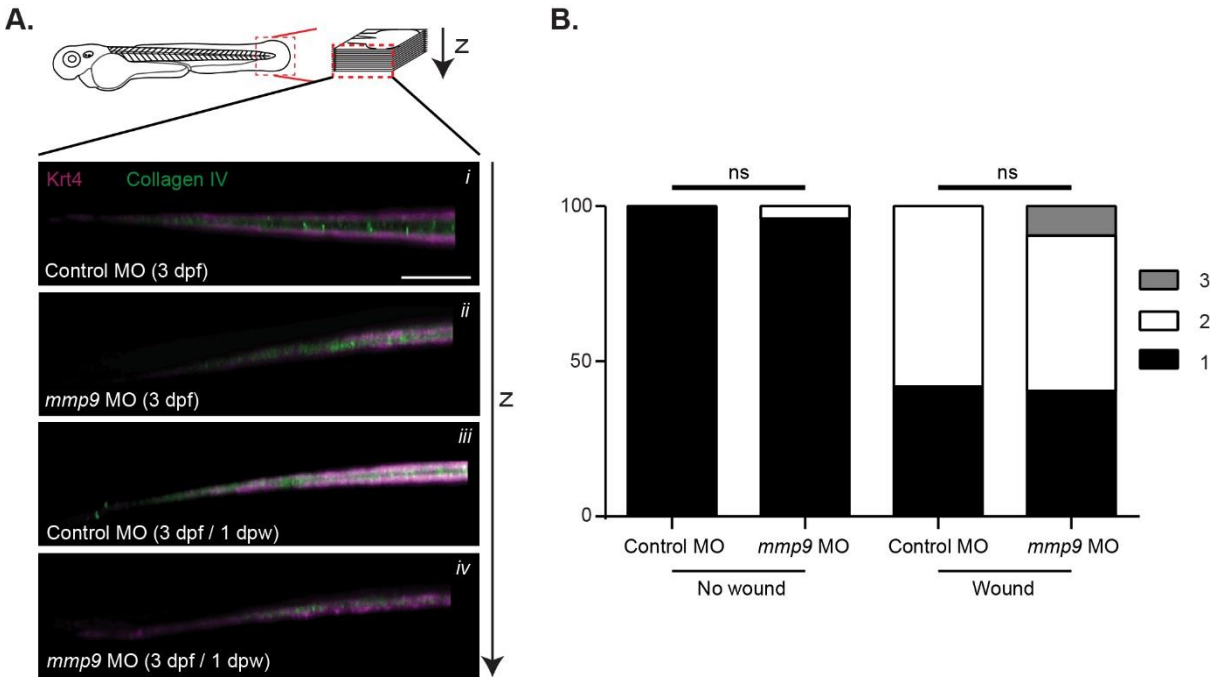

Fig. S3. No defects in collagen type IV (IHC) or alignment of collagen fibers are observed at 2 dpw. A) Antibody labeling (IHC) of type IV collagen did not yield obvious differences between the different conditions. B) Blind analysis for collagen alignment (SHG) at 2 dpw indicated a non-significant increase in collagen mis-alignment in both control and *mmp9* morphant caudal-fins. Graph represents data from experiments performed in quadruplicate and scored by an individual, single-blind analyzer. Scale bar in A represents 50 µm. Graph represents pooling with experimental numbers for no wound Control MO = 21, no wound *mmp9* MO = 25, wounded Control MO = 31, wounded *mmp9* MO = 32.

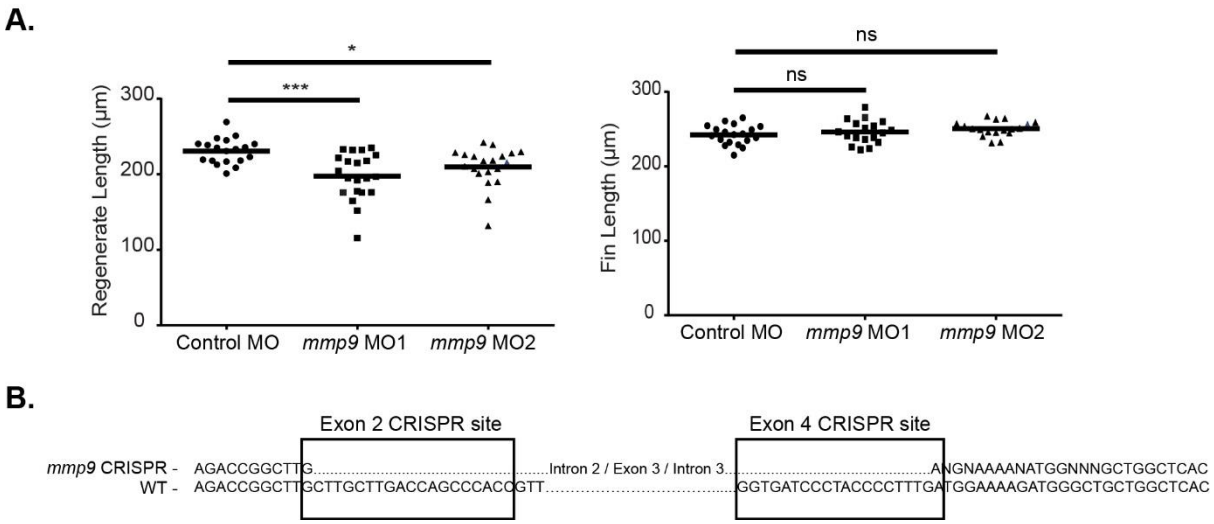

Fig. S4. The wound healing defect in Mmp9-deficient larvae at 3 dpw is not due to an early reduction in leukocyte recruitment. A) Both *mmp9* MOs resulted in a significant wound-healing defect at 3 dpw (5 dpf) while having no influence on developmental fin length at 5 dpf. B) Sequencing verification of two-site *mmp9* CRISPR- Cas9 amplicon. Statistical significance: * P<0.05 and *** P<0.001. Graphs represent a single experiment performed in triplicate.

Movie 1. 3D reconstruction of SHG imaging of control caudal-fin. Rotating 3D reconstruction, generated using Bitplane Imaris software, of SHG in a control caudal-fin. Initial rotation shows reconstruction of SHG image data, with subsequent rotation showing 3D surface rendering of this data, illustrating the three-dimensional organization of the collagen fibers. Note the space formed between the dorsal and ventral layers of collagen fibers. Image collection performed as for Figure 3B.

Movie 2. 3D reconstruction of SHG imaging of *hai1* morphant caudal-fin. Rotating 3D reconstruction, generated using Bitplane Imaris software, of SHG in a *hai1* morphant caudal-fin. Initial rotation shows reconstruction of SHG image data, with subsequent rotation showing 3D surface rendering of this data, illustrating the three-dimensional organization of the collagen fibers. Note the space formed between the dorsal and ventral layers of collagen fibers. Image collection performed as for Figure 3B.

Movie 3. 3D reconstruction of SHG imaging of *hai1 + mmp9* morphant caudal fin. Rotating 3D reconstruction, generated using Bitplane Imaris software, of SHG in a *hai1 + mmp9* morphant caudal-fin. Initial rotation shows reconstruction of SHG image data, with subsequent rotation showing 3D surface rendering of this data, illustrating the three-dimensional organization of the collagen fibers. Note the space formed between the dorsal and ventral layers of collagen fibers. Image collection performed as for Figure 3B.